Optics Letters

Broadband extreme ultraviolet dispersion measurements using a high-harmonic source

G. S. M. Jansen,[1,2] X. Liu,[1,2] K. S. E. Eikema,[1,2] and S. Witte[1,2,*]

[1]Advanced Research Center for Nanolithography (ARCNL), Science Park 106, 1098 XG Amsterdam, The Netherlands
[2]LaserLaB, Department of Physics and Astronomy, Vrije Universiteit, De Boelelaan 1081, 1081 HV Amsterdam, The Netherlands
*Corresponding author: witte@arcnl.nl

Received 22 May 2019; revised 21 June 2019; accepted 21 June 2019; posted 24 June 2019 (Doc. ID 368179); published 18 July 2019

We demonstrate direct dispersion measurements of various thin films at extreme ultraviolet (EUV) wavelengths, using a table-top laser-driven high-harmonic generation (HHG) source. In this method, spatially separated identical EUV pulses are generated through HHG with a pair of phase-locked infrared pulses. The EUV pulses are re-imaged to a sample plane using a single toroidal mirror, such that one pulse illuminates the target thin film, while the other pulse passes through a reference aperture. By comparing the EUV interference with and without a sample, we are able to extract the dispersion properties of the sample, integrated over the full film thickness. We have measured thin films of titanium, nickel, copper, and silicon nitride, demonstrating that this technique can be applied to a wide range of materials, only requiring a film thin, enough for sufficient EUV transmission.

https://doi.org/10.1364/OL.44.003625

Accurate knowledge of dielectric constants is crucial for the determination of the optical response of materials. Recently, the development of extreme ultraviolet (EUV) lithography and the widespread availability of EUV light sources for scientific and technological purposes have sparked an increased interest in dielectric constants at EUV wavelengths [1–3]. A major source of dielectric constants and related material properties is the x-ray database compiled by the Center for x-Ray Optics (CXRO), which is based on the work of Henke *et al.* [4]. In this database, atomic scattering factors are used to derive optical properties such as the refractive index, absorption length, and reflection coefficient. While this provides excellent results for a large part of the spectrum, it is somewhat limited in the EUV range (10–124 eV, 124–10 nm). In particular, being purely atomic scattering data, it does not account for any structural or molecular effects which may be relevant for these low energies, leading to possible discrepancies [5]. Furthermore, the real part of the atomic scattering factor has not been tabulated below 30 eV, so that optical properties of materials in that wavelength range remain undetermined.

There have been several efforts towards the measurement of dielectric constants in the EUV regime, typically using a synchrotron or high-harmonic generation (HHG) sources of EUV light. For example, in angle-resolved reflectometry, the reflectance from a thin film is measured for a range of angles [6–9]. Film parameters such as the complex refractive index, density, thickness, and roughness can then be retrieved by fitting the data to a suitable model. This measurement is typically performed for many incident photon energies. A similar approach has been used to retrieve the refractive index from the forward scattering or diffraction of the nanoparticles [10]. Another approach to measuring the complex refractive index employs the Kramers–Kronig relationship. Based on an the accurate measurement of the energy-dependent absorption, these relations can be used to calculate the full refractive index [11–13]. A more direct approach to measuring the refractive index and absorption of a material is based on interferometry [14]. In such experiments, the transmission of a thin film is made to interfere with a reference wave. The refractive index and absorption can be retrieved directly from the interference phase and amplitude, respectively.

In this Letter, we present a novel implementation of an ultra-broadband interferometric EUV dispersion measurement, based on Fourier-transform spectroscopy (FTS). To this end, we use two independently generated, but phase-locked, sources of HHG that function as a probe and reference. We ensure sub-attosecond accurate timing (therefore, phase) control through the use of a birefringence-based common-path interferometer [15]. By scanning the relative phase between the sources, we are able to measure the wavelength dependence of the sample-induced phase over the full HHG spectrum in a single measurement. The measurement geometry is simple and versatile, and the setup is of table-top size. The presented approach directly measures the optical path length through the sample Therefore, it is much more robust against surface effects such as roughness or oxidation, compared to reflection-based measurements [8,9]. It does not require variation of the angle-of-incidence, and it works independently of the EUV spectrum produced by the HHG source.

For our experiments, we use the output of a titanium-sapphire-seeded non-collinear optical chirped pulse amplifier. This system provides 8 mJ pulses with a 25 fs duration, has a spectrum centered on 840 nm wavelength, and has a repetition rate of 300 Hz. These pulses are split into pairs of identical pulses with a controllable and intrinsically stable delay, using an

interferometer based on birefringent wedges [15]. After the interferometer, the pulse pairs are focused in a gas jet for HHG. In the gas jet, the individual pulses are spatially separated by approximately 300 μm by applying a small tilt to the final wedge in the interferometer. This ensures that both pulses generate high harmonics independently. In order to get a spectrum covering the EUV regime, we generate high harmonics in neon gas. We use a 200 nm thick, free-standing aluminum filter to separate the EUV from the driving infrared radiation. Behind the filter, we observe a spectrum of the 17th up to the 49th harmonic, spanning from 50–17 nm (25–72 eV).

After the HHG, the two EUV beams diverge, so that they overlap and interfere in the far field. In order to separate probe and reference for the refractive index measurement, we use a boron-carbide (B_4C) coated toroidal mirror with a 7.5° grazing incidence angle and a 25 cm focal length to re-image the HHG sources to the sample plane. At this grazing incidence angle, the boron-carbide is expected to have a high reflectivity of up to 80% without a strong wavelength dependence. The spectra observed after the toroidal mirror agree with this expectation.

In the sample plane [Fig. 1(a)], we use a three-dimensional piezo-driven translation and rotation stage (SmarAct) to position a mask with a sample and a reference aperture. This mask consists of a 15 nm thin, 250 by 250 μm wide silicon nitride membrane. The membrane is partially coated with a 100 nm gold layer, ensuring that it is opaque for EUV radiation, except for one corner of the membrane which is not coated with gold. We then deposited a thin layer of the material to be investigated over the full membrane, so that in the corner without gold only the material under investigation is deposited, while the rest of the membrane is opaque due to the gold layer. Finally, we used focused ion-beam milling to clear an aperture in the opposite corner of the membrane. Therefore, the mask consists of two transmitting regions: (1) the sample corner, consisting of either 15 or 50 nm silicon nitride and for example 25 nm of titanium; (2) a reference aperture, typically a circular hole of 10 μm diameter.

After the sample, the beams diverge again and overlap in the far field. There the detected signal at position $\vec{r}$ on the detector $S(\vec{r}, \lambda, \Delta t)$ consists of the coherent addition of the probe E_p and reference E_r beam:

$$S(\vec{r}, \lambda, \Delta t) = \int |E_p(\vec{r}, \lambda, t) + E_r(\vec{r}, \lambda, t - \Delta t)|^2 \mathrm{d}t. \quad (1)$$

As the detector receives the full source spectrum, a measured interference pattern at a given time delay Δt is the integral of Eq. (1) over all wavelengths λ present in the illumination. Note that in this Letter, we write λ for the wavelength in vacuum. Integrating Eq. (1) over time, the signal for a single wavelength λ can be written as

$$S(\vec{r}, \lambda, \Delta t) = |A_p(\vec{r})|^2 + |A_r(\vec{r})|^2 + A_p(\vec{r})A_r(\vec{r}) \times \exp[i(2\pi c \Delta t/\lambda + \Delta\Phi(\vec{r}, \lambda))] + \text{c.c.}, \quad (2)$$

where A_p and A_r are the amplitudes of the probe and reference beams, respectively, and $\Delta\Phi$ is the phase difference between the beams. An FTS measurement consists of a series of intensity measurements over a range of delays. As the contribution for every wavelength λ oscillates at its characteristic frequency $2\pi c/\lambda$, a Fourier transform over the time domain can be used to extract the relevant part of the measured signal:

$$M(\vec{r}, \lambda) = A_p(\vec{r})A_r(\vec{r}) \exp(i\Delta\Phi(\vec{r}, \lambda)). \quad (3)$$

The settings for the FTS scan are optimized for the characteristics of the HHG spectrum. As the shortest wavelength is 17 nm, the delay step between measurements must be at least smaller than 8.5 nm. Typically, a delay step of 5 nm was used. The length of the delay scan is set by the desired spectral resolution. We typically used a scan length of 3.1 fs, which provides sufficient spectral resolution to resolve the individual high harmonics, while still keeping the total measurement time relatively short at a 15 min per delay scan.

The phase difference between the probe and reference contains several contributions. In general, the phase difference $\Delta\Phi$ is the sum of the sample-induced phase $\Phi_{\text{sample}}(\lambda)$, a geometry-related phase $\Phi_{\text{geo}}(r, \lambda)$, and any phase variation $\Phi_{\text{HHG}}(r, \lambda)$ arising from the HHG itself. For a simple multilayer sample, we approximate the sample phase as the sum of the optical path length differences induced by the materials:

$$\Phi_{\text{sample}}(\lambda) = \sum_i \frac{n_i(\lambda) d_i}{\lambda}, \quad (4)$$

which contain the individual wavelength-dependent refractive indices $n_i(\lambda)$ and thicknesses d_i. For such thin films, care should be taken that possible multilayer interference effects are properly taken into account: we have also performed simulations using the Fresnel theory and found that for our simple, strongly absorbing layer structures the approximation of Eq. (4)

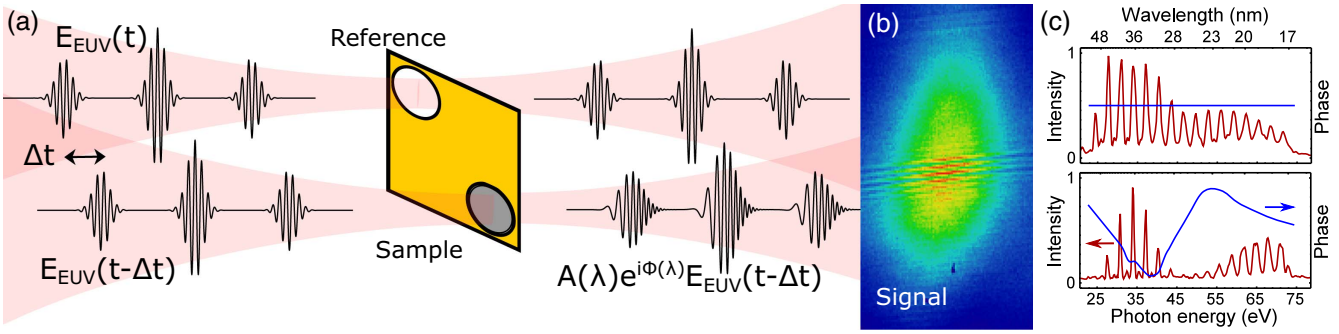

Fig. 1. Schematic overview of the EUV interferometry for dispersion measurements. (a) From the left, two identical EUV pulses are imaged to a mask with a reference aperture and sample aperture. (b) The sample modulates the incident pulse in phase and amplitude, which is visible in the far-field interference on the camera. By scanning the delay between the beams, we perform FTS. (c) Typical spectral intensities (red) and relative phase between the pulses (blue) as measured without a sample (top) and a spectrum as measured with 30 nm thick titanium sample (bottom).

is accurate to within a few milliradians. For our planar samples, the sample-induced phase has no transverse spatial dependence. The geometric phase is determined by the optical path length difference between the beams, arising from the source geometry and refocusing optics, and does not depend on the presence of a sample. As the two EUV beams are generated in separated spots, the geometric phase is dominated by a linear phase ramp leading to a Young's double slit-type interference pattern [Fig. 1(b)]. In addition to the linear phase ramp, the geometric phase also contains a higher-order spatial structure originating from the toroidal mirror aberrations. The two EUV beams have a slightly differing incidence angle on the toroidal mirror, which leads to a difference in astigmatism between the beams. Such aberrations can be reduced using a pair of toroidal mirrors [16] but, in our experiment, all geometry-induced phase effects are removed through a calibration measurement, as detailed below. Finally, it is possible that there are phase differences arising from the HHG. While the two HHG sources are optimized to be identical, slight differences cannot be excluded. In particular, differences in gas pressure and spatial and temporal chirp of the driving pulses may lead to a phase difference, depending on position and wavelength. A systematic offset between the two sources can be removed, similar to the geometric phase, but variations during the measurements can be a source of fluctuations in the retrieved phase signal.

In order to extract the sample-induced phase, we perform a series of three measurements: (1) a reference measurement M_{ref} without a sample in either beam, (2) a measurement M_{sample} with the sample in one of the beams, and (3) an "inverse" measurement with the sample rotated by 180°, interchanging the role of sample and reference beams. By multiplying the result of the sample measurement with that of the conjugate reference measurement, we get

$$M_{\mathrm{sample}}(\vec{r})M^{*}_{\mathrm{ref}}(\vec{r}) = A_r^3(\vec{r})A_p(\vec{r})\exp(i\Phi_{\mathrm{sample}}(\lambda)), \quad (5)$$

which subtracts the geometric and HHG phase from the measurement. We then apply an intensity threshold, ensuring that only those pixels and wavelengths with a sufficient signal-to-noise ratio are included in the final phase determination. Finally, we extract the phase as a function of the wavelength, integrated over the position to improve the signal-to-noise ratio. This analysis procedure is performed for the rotated sample geometry as well, after which the average of the analysis results for both geometries is taken to eliminate the influence of possible differences between the EUV beams.

Presently, the reproducibility of the interferometer used in the FTS scans forms the main technical limitation to the experimental accuracy. We typically observe slight variations of the absolute interferometer arm lengths between individual scans, resulting in an arbitrary time delay variation of ~100 as from one scan to the next. After the analysis described above, using Eq. (5), such a variation corresponds to 30 nm in optical path length and 0.1 rad/PHz in phase slope. As this variation is random, the measurement accuracy can be further improved by averaging multiple measurements. In our present system, this procedure results in an expected accuracy for the phase slope at the 10^{-2} rad/PHz level, but hampers the retrieval of the absolute phase delay introduced by the sample for a sufficiently accurate refractive index determination. Nevertheless, with a better translation stage in the FTS scan, this would become possible. As this was not available, we have instead focused on the relative phase influence and determined the group-delay dispersion (GDD) from it.

We have measured the sample-induced phase for four different samples: a 25 nm titanium film, a 40 nm nickel film, both sputter coated on 15 nm silicon nitride membranes, a 30 nm copper film on a 50 nm silicon nitride membrane, and a bare 50 nm silicon nitride membrane. For every sample, we performed several measurement series. The results from these measurements and comparisons with the expected phase delay from CXRO data are shown in Fig. 2. We performed the sample and reference measurements sequentially, consisting of FTS scans with and without a sample. These measured dispersion data are corrected for the global phase offset arising from the uncertainty in the absolute timing between the beams. We do this by adding a constant phase to the measured phase curves shown in Fig. 2 to facilitate a comparison of the measured data with the CXRO expectation.

The observed spectral phase dependence follows the reported literature curves to within the measurement accuracy, and our measurements extend the dispersion data for Ti and Si_3N_4 down to 20 eV photon energy. For the titanium dataset, we found that the measured phase had a smaller wavelength-dependent variation than initially expected based on the assumption that the titanium film was 25 nm thick, hinting to a lower film thickness. Therefore, we performed a least-squares fit of the data to the CXRO model using the titanium

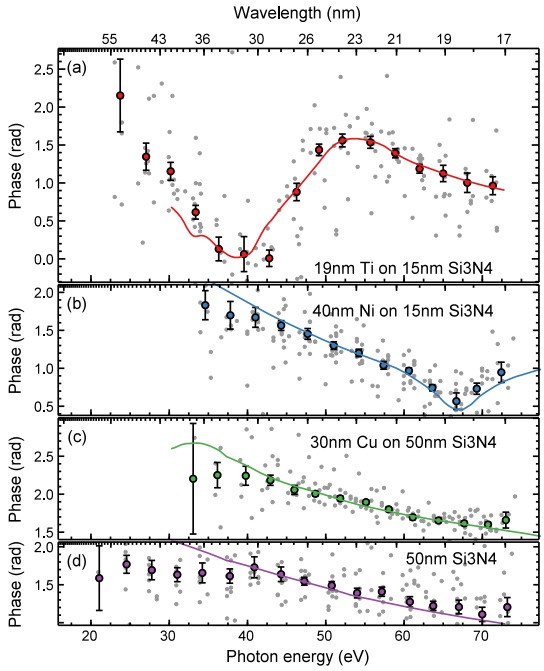

Fig. 2. Measured phase induced by various metal films on silicon nitride: (a) titanium, (b) nickel, (c) copper, and (d) bare Si_3N_4. The individual measurement points are shown in gray, while the colored points show the mean phase and standard deviation of the mean for each harmonic. The lines show the prediction for 30 eV and higher energies based on CXRO values for the refractive index. For titanium, the thickness was determined to be 19.0 ± 1.6 nm titanium on 15 nm silicon nitride based on a fit of the data. For nickel and copper, the transmission at energies below 35 eV was insufficient for a phase measurement. No CXRO data are available for photon energies below 30 eV.

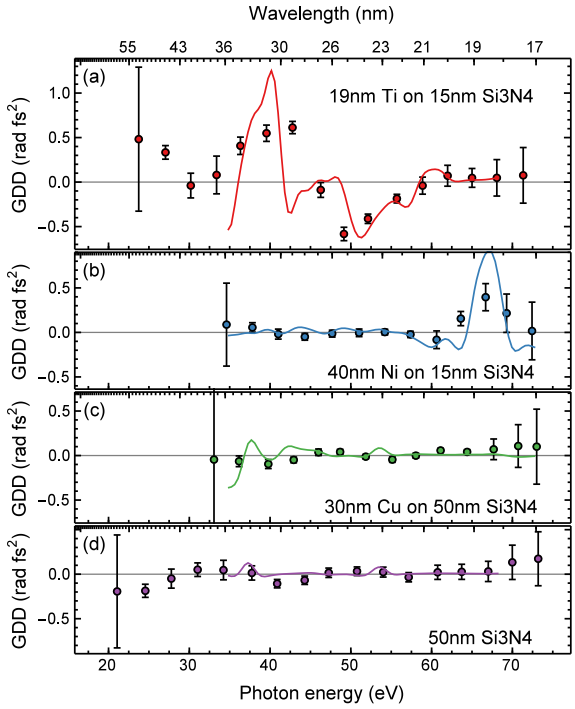

Fig. 3. GDD retrieved from the data of Fig. 2 for (a) titanium, (b) nickel, (c) copper, and (d) bare Si_3N_4 (filled points), along with the GDD as calculated from CXRO reference data (solid lines).

layer thickness as a free parameter. This fit resulted in a layer thickness of 19.0 ± 1.6 nm, which is within the uncertainty range and calibration accuracy of the fabrication process. Similar agreement between measurement and expectation is found for nickel, copper, and silicon nitride, although the linear component of the phase slightly differs from the expectation. For silicon nitride, where this difference is the largest, the deviation is roughly 0.04 rad/PHz, which is still in the range of expected variation due to the interferometer repeatability. Both nickel and copper suffer from strong absorption at low photon energy, which limited the observable interference to the 35–72 eV spectral region and results in increased error bars towards lower energy.

Higher-order dispersion properties are not influenced by the absolute timing uncertainty in the measurement and, therefore, can be determined in an absolute sense. Figure 3 shows the GDD across the full spectral range as retrieved from the measured data. The results mostly agree with reference data within the statistical measurement accuracy of typically 0.1 rad fs^2, with some deviations at the positions of strong spectral variation, which may be improved by denser spectral sampling.

As discussed above, the main error source in these measurements comes from the interferometer reproducibility between sample and reference measurements. Improving the absolute timing reproducibility between the interferometer arms to 5 attoseconds would enable a determination of the optical path length of a sample with 1.5 nm accuracy from a single scan. This corresponds to an absolute phase accuracy of 5% at 30 nm wavelength and an accuracy for the group delay of 5 mrad/PHz, which goes beyond any other method for dispersion measurements in this soft x-ray wavelength range, and would enable full complex refractive index determination.

In this experiment, we measured dispersion averaged over the spatial domain for thin films. Furthermore, this approach can be combined with Fourier-transform holography [17], enabling dispersion mapping with nanometer-scale spatial resolution. Another potential application is the characterization of EUV multilayer mirrors, which can be used to control the spectral phase of high harmonics [18]. The spectral range was determined by the HHG source and the Al filter, but the FTS-based interferometry approach is compatible with more complex and even continuous EUV source spectra. Therefore, the method can readily be extended in a spectral range through the combination with, e.g., few-cycle driving pulses [19], mid-IR drivers [20], or optical gating [21] combined with different filters.

Funding. H2020 European Research Council (ERC) (ERC-StG 637476); Nederlandse Organisatie voor Wetenschappelijk Onderzoek (NWO).

REFERENCES

1. R. Soufli and E. M. Gullikson, Proc. SPIE **3113**, 222 (1997).
2. E. Louis, A. E. Yakshin, T. Tsarfati, and F. Bijkerk, Prog. Surf. Sci. **86**, 255 (2011).
3. Y.-S. Ku, C.-L. Yeh, Y.-C. Chen, C.-W. Lo, W.-T. Wang, and M.-C. Chen, Opt. Express **24**, 28014 (2016).
4. B. L. Henke, E. M. Gullikson, and J. C. Davis, At. Data Nucl. Data Tables **54**, 181 (1993).
5. C. T. Chantler, J. Phys. Chem. Ref. Data **24**, 71 (1995).
6. C. Tarrio, R. N. Watts, T. B. Lucatorto, J. M. Slaughter, and C. M. Falco, Appl. Opt. **37**, 4100 (1998).
7. H. Y. Kang, J. D. Lim, P. Peranantham, and C. K. HwangBo, J. Opt. Soc. Korea **17**, 38 (2013).
8. R. Soufli and E. M. Gullikson, Appl. Opt. **36**, 5499 (1997).
9. D. L. Windt, W. C. Cash, M. Scott, P. Arendt, B. Newnam, R. F. Fisher, A. B. Swartzlander, P. Z. Takacs, and J. M. Pinneo, Appl. Opt. **27**, 279 (1988).
10. B. Mills, C. F. Chau, E. T. F. Rogers, J. Grant-Jacob, S. L. Stebbings, M. Praeger, A. M. de Paula, C. A. Froud, R. T. Chapman, T. J. Butcher, J. J. Baumberg, W. S. Brocklesby, and J. G. Frey, Appl. Phys. Lett. **93**, 231103 (2008).
11. B. Kjornrattanawanich, D. L. Windt, J. A. Bellotti, and J. F. Seely, Appl. Opt. **48**, 3084 (2009).
12. B. Sae-Lao and R. Soufli, Appl. Opt. **41**, 7309 (2002).
13. Y. A. Uspenskii, J. F. Seely, N. L. Popov, A. V. Vinogradov, Y. P. Pershin, and V. V. Kondratenko, J. Opt. Soc. Am. A **21**, 298 (2004).
14. C. Chang, E. Anderson, P. Naulleau, E. Gullikson, K. Goldberg, and D. Attwood, Opt. Lett. **27**, 1028 (2002).
15. G. S. M. Jansen, D. Rudolf, L. Freisem, K. S. E. Eikema, and S. Witte, Optica **3**, 1122 (2016).
16. L. Poletto, F. Frassetto, F. Calegari, S. Anumula, A. Trabattoni, and M. Nisoli, Opt. Express **21**, 13040 (2013).
17. R. L. Sandberg, D. A. Raymondson, C. La-o vorakiat, A. Paul, K. S. Raines, J. Miao, M. M. Murnane, H. C. Kapteyn, and W. F. Schlotter, Opt. Lett. **34**, 1618 (2009).
18. M. Hofstetter, M. Schultze, M. Fieß, B. Dennhardt, A. Guggenmos, J. Gagnon, V. S. Yakovlev, E. Goulielmakis, R. Kienberger, E. M. Gullikson, F. Krausz, and U. Kleineberg, Opt. Express **19**, 1767 (2011).
19. F. Ferrari, F. Calegari, M. Lucchini, C. Vozzi, S. Stagira, G. Sansone, and M. Nisoli, Nat. Photonics **4**, 875 (2010).
20. T. Popmintchev, M.-C. Chen, P. Arpin, M. M. Murnane, and H. C. Kapteyn, Nat. Photonics **4**, 822 (2010).
21. H. Mashiko, S. Gilbertson, C. Li, S. D. Khan, M. M. Shakya, E. Moon, and Z. Chang, Phys. Rev. Lett. **100**, 103906 (2008).